International Conference on Space Optics—ICSO 2022

Dubrovnik, Croatia

3–7 October 2022

Edited by Kyriaki Minoglou, Nikos Karafolas, and Bruno Cugny,

Active optics for the DICOS project

Active optics for the DICOS project

J.M. Le Duigou[1], L. Bernard[2], M. Castelnau[1], E. Cucchetti[1], C. Latry[1], M. Soulier[1,3], A. Salih Alj[1,4]

[1]CNES, 18 avenue Edouard Belin, 31400 Toulouse, France; [2]MAGELLIUM, Parc technologique du Canal, 1, rue Ariane 31520 Ramonville Saint-Agne, France; [3]INSA Toulouse,135 avenue de Rangueil 31077 Toulouse CEDEX 04, France, [4]Institut Supérieur de l'Aéronautique et de l'Espace, 10, avenue Edouard Belin - BP 54032, 31055 Toulouse Cedex, France

ABSTRACT

DICOS is a technological demonstrator for a future space-based small optical telescope based on active optics and with high stability requirements. It belongs to a new CNES set of programs called "EXperimental Projects" (PEX). It favors fast developments with breaking technology to be demonstrated in a representative object but without applying the full set of space constraints. The current phase of DICOS is to build a ground-based prototype and test it by the end of 2024. It will then be adapted to fly under a stratospheric balloon and demonstrate its compatibility with conditions close to the space ones. The instrument uses a full aluminum 40 cm off axis telescope of the Cassegrain type with an optical bench behind the primary. The machining and the assembly tolerances are relaxed but compensated by active optics. The secondary mirror is mounted on a six degrees of freedom device that performs the coarse alignment. Then, an active closed optical loop located inside the optical bench corrects the surface error of the mirrors as well as the thermoelastic variations of the telescope. The goal is to reach a 20 nm rms wavefront error (WFE) for spatial frequency lower than 5 cycles/pupil diameter, stable to 1 nm rms and with a 0.01 Hz sampling frequency. The sizing case was taken from the field of coronography for exo-planets direct detection. This paper first presents a brief summary of the DICOS project. Then we report the excellent performances obtained experimentally on the active loop. It currently manages to reduce an initial 400-500 nm rms WFE (from Z4 to Z36) down to a few nm in 3-4 iterations of about 40 s each. We also present a detailed characterization of the DM and some recent efforts to demonstrate its compatibility with vacuum and thermal loading.

Keywords: Fine pointing, wavefront control, active optics, coronography, stratospheric balloon, CARMEN

1. INTRODUCTION

Since 2010, CNES develops its activities in the field of active optics for future space based missions.

In the frame of the Earth observation field, the OTOS/TANGO technological program paved the way for a future in orbit large and very compact telescope using active optics[1]. This program included various studies and breadboards both at CNES and in the industry to develop some of the critical building blocks, like the deformable mirrors (DM)[2,3], the wavefront sensors[4], extremely lightweight mirrors,... It ended up recently by a full-scale demonstrator made by TAS under a CNES contract[5]. For this kind of application, the DM only requires a few tens of actuators to correct the low spatial frequencies of the telescope point spread function (PSF). Furthermore, it has to be located in a pupil plane of the optics as the instrument usually has a quite large field of view.

In parallel, in the astronomy domain, CNES supported R&D activities in associated French laboratories and research centers like LESIA, LAM, OCA or ONERA to develop the technology of coronography for the direct detection of exo-planets. Extremely high contrast in a so-called "Dark hole (DH)" also requires the use of active optics, but with much more actuators than in the previous case (few 1000's). The best result (few 10^{-9} 1 σ contrast @ 5 λ/D) was achieved at LESIA[6] on the THD2 breadboard in monochromatic light using a four quadrant phase mask (4QPM)[7] combined with an AO loop based on the self-coherent camera as a wavefront sensor[8] and two Boston Micromachine 32x 32 DMs. In this case, as

extreme stability is required, it is very important to have the wavefront sensing using directly the science image to avoid the non-common paths. Very fine pointing is also required to a level of few mas on the sky with high bandwidth.

A simplified copy of the THD2 breadboard called IHDC was implemented in the optical laboratory of the Toulouse Space Center to study the stability conditions required by such ambitious concepts. With moderate efforts and a strong support of LESIA, we could implement in a few years (2014-2018) the fundamental principles of the THD2 dealing only with the phase aberrations in monochromatic light with a 4QPM coronograph. We could reach about 10^{-7} average contrast and few 10^{-8} 1 σ contrast in a half DH in the range of 5 to 10 λ/D, bringing a strong confirmation of the principles developed at LESIA[9].

These excellent results combined with the recalled context on active optics encouraged us to propose a technological small mission to demonstrate the feasibility in space of such ambitious stability requirements. We started from the coronography application, but the targeted performances could be useful for many other missions. A short study ruled out a space mission because of its much too high cost. A balloon-borne instrument appears more affordable and the idea to start a project on this basis was accepted early 2020.

CNES has been using stratospheric balloons for more than 60 years and has a large experience in this field. Since 2014, 27 successful flights of heavy zero pressure balloons have been carried out from various launch sites[10]. They are often used as an intermediate step before considering a space mission and are very useful to test new technologies or concepts in quasi-space conditions. CNES recently participated to the FIREBALL[11] mission (inter-galactic medium in the UV) in cooperation with the US with the third launch now planned at Fort Sumner in late 2022. Following the experience gained on fine pointing issues during this mission[12,13], the CNES balloon team wishes to improve the pointing accuracy of its systems to provide an enhanced service to its customers. DICOS is for them an excellent opportunity.

Last, DICOS is made possible by a new framework at CNES, called the "PEX". It is a funding line dedicated to experimental demonstrations of advanced instrumental concepts in representative conditions. The goal is to aim quick developments relying on experimentation and empirical approach with limited funding and human resources. The management of such projects is minimized and has not the burden of true space projects allowing agility. The PEX only covers the first part of the project (DICOS-1) limited to a ground demonstration (expected end 2024). We plan a second part (DICOS-2) that will take into account more constraints due to the balloon environment and will hopefully lead to a real flight.

2. DICOS SHORT DESCRIPTION

See a CAD overview of the instrument inside its gondola on fig. 1. More details can be found in a previous publication[9].

Figure 1. CAD view of DICOS inside the CARMEN gondola

2.1 The instrument

Fig. 2 gives an overview of the instrument mounted on its mobile testing stand. All the main components are now in the manufacturing phase or already procured.
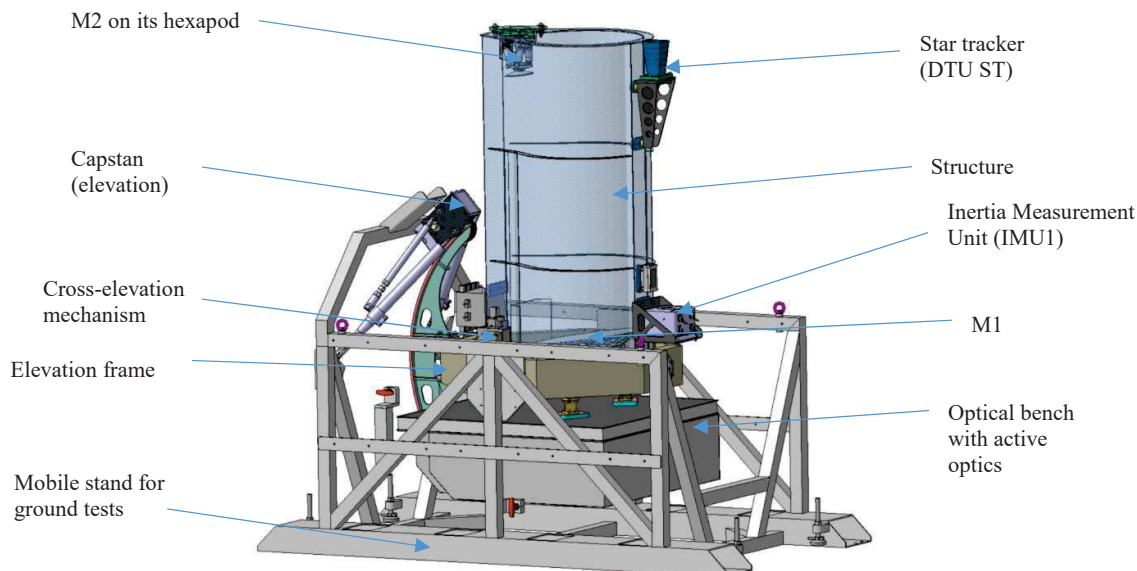

Figure 2. The DICOS instrument on its mobile stand

The instrument optical design is driven by the use of active optics to relax the constraints as much as possible and obtain a low cost solution for the mirrors and the structure. We choose to push this strategy to its maximum using a full aluminum telescope, with high thermal deformations, but close to the homothetic case.

Figure 3. M1 design

The M1 and M2 mirrors form an off axis Cassegrain-type telescope with D=40 cm and f~6.4m. The size along the pointing axis is limited by the accessible space in the CARMEN gondola and the M1/M2 distance is close to 1 m. The entrance pupil is on the M1. The maximal FOV is 18 arcmin for the guiding channel but limited to 3 arcmin in the main channel. The mirrors are made of a special aluminum alloy (RSA905). Recent improvements on the precise machining and polishing allow using this kind of solution without adding a Ni based layer to reach better than 5 nm rugosity and 100 nm WFE. The mechanical design of the mounting points allows a very high filtering of the interface deformations.

The intermediate focus is located just at the entrance of the optical bench. A six degrees of freedom (DoF) mechanism supports the M2 for rough alignment purposes and compensation of the ground/flight deformation. It is a PI H-811.I2V standard device.

The structure is based on a 2 mm thick aluminum tube designed to support the mirrors, the star tracker, its driving electronics, the inertia measurement unit and one of the on board computer. Due to the presence of the mechanism under M2, the tolerances on the structure are quite relaxed (0.1 mm class) except for the interface plane of the M1. The tube is fixed on a 2 cm thick baseplate carrying the M1. The link with the gondola or with the testing stand is made through an elevation frame. The location of the star tracker is imposed at the top of the instrument for field of view reasons. The angle bias with the main optical channel due to alignment and thermal variations can be as much a 10 arcmin, This imposes a guiding channel.

The general size of the instrument is about 1 x 1 x 2 m. The total weight of the mobile part is about 150 kg with a maximum inertia close to 25 m^2.kg. The first mode of the mobile part is slighlty above 30 Hz. This is imposed to avoid instability of the pointing control. The passive thermal control is designed to have M1 above -40°C in flight with very low in plane gradient. The impact of temperature changes are minimized by the homothetic design.

The optical bench structure (0.9 x 0.9 x 0.055 m) is an adaptation of a PGB-SP0164 Thorlabs aluminum honeycomb bench. It has a 60 mm diameter hole to let the optical beam enter. It carries all the relays optics to feed four channels: a guiding channel (CAM0, f/#=11), a fine pointing camera (CAM1, f/#=22), a camera for the phase diversity (CAM1B, f/#=50), a control camera (CAM2). The set up uses either spatial or spectral separation. See fig.4.
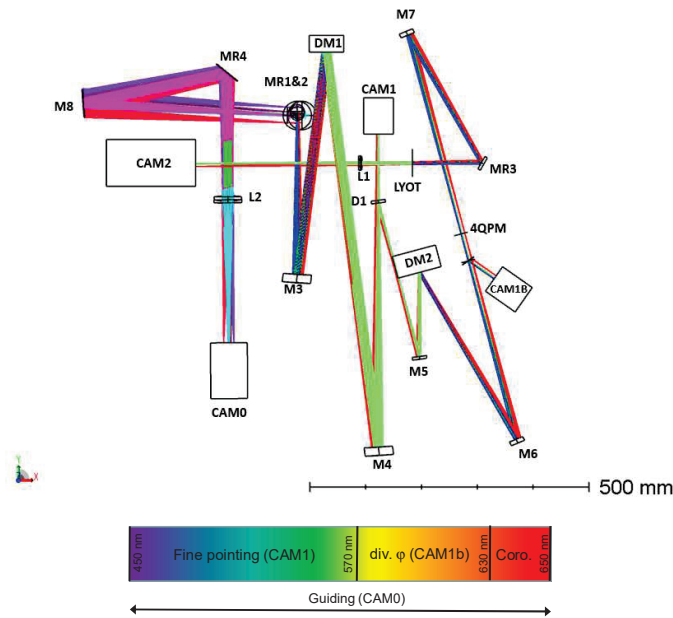

Figure 4. Optical bench design and spectral bands

The core of the optical bench is the ALPAO DM97-25 (DM1, pupil size 22.5 mm, 97 actuators). It is located in the pupil plane conjugated to M1 by M2 and M3. In the long term, DM2 could be a DM with a high number of actuators to create a DH. For the first versions of DICOS, it will only be a flat mirror and the 4QPM channel is only implemented to verify that the stabilization conditions are met. The total weight of the optical bench is close to 50 kg. Its first mode when mounted on its three interface blades is above 80 Hz. The optical bench is thermally controlled by heaters and adapted insulation layers and cover to maintain an average temperature of 20°C +/- 1°C.

2.2 The gondola

We plan to use the standard CARMEN gondola in a configuration with DICOS as the only payload. See the illustration on fig. 1. It is a truss structure made of aluminum that can support as much as 800 kg in a volume less than 4 m^3. The upper main structural beam provides the interface with the balloon flight chain. The internal space where the instrument can be accommodated has a maximum height of about 2 m and a width of 1.2 m. The instrument with its elevation frame can either be directly mounted on the walls with interface plates as on fig.1 but we might also embark the mobile stand used for the instrument testing and use it for stiffening the gondola walls (see fig. 2).

The center of gravity (CoG) of the mobile part has to be collocated with the intersection of the elevation/cross elevation axis within few mm accuracy after the assembly. To achieve this, the instrument is designed to reach about 1 cm maximal CoG offset and the final adjustment is made by adding small masses to fine-tune the balance of the mobile part. The CoG shall also be located on the axis of the balloon flight chain. The CARMEN walls will be used to accommodate all the avionics electronics and the eight batteries.

2.3 The pointing system

The pointing of DICOS relies on a three stages architecture. See fig.5. The stage #1 (coarse) is the gondola azimuth control. The stage #2 (fine pointing) uses Elevation (E) and Cross-elevation (CE) control of the instrument. The stage #3 (or very fine pointing) is based on small tip and tilt actuations of the DM located inside the optical bench. The first and second pointing stages use the FIREBALL mission legacy[12,13]. For DICOS, only the line of sight (LOS) is controlled and no field rotation control is performed.

The azimuth of the gondola is controlled using a torque motor with velocity and torque feedback, attitude and velocity feedback from an inertia measurement unit on the floor of the gondola (IMU0). The platform itself is stabilized thanks to two reaction wheels (RW) located in the walls of the gondola. For the fine pointing, the elevation frame rotates around the elevation axis. It is driven by a capstan and wheel system (see fig. 2) that allows 0-90° elevation. The frame carries the driving mechanism for the cross elevation that allows a +/-3° stroke. It is based on a brushed direct current motor with an appropriate lever of arm. The outputs of the IMU1 and the DTU star tracker located on the instrument are fused into a gyro-stellar constant gain Kalman filter estimating the LOS quaternion and the three axis gyro drifts from IMU1. For the very fine pointing, a precise centroid position of the target star is obtained by a robust barycentric computing from a camera located in the optical bench (CAM1) on a 50 px wide window. This algorithm is built on the legacy of the ESTADIUS system[14] used successfully on the PILOT mission. It can reach as much as 500 Hz sampling frequency, that is required to reject the 0.5 Hz 1'' residual of the second stage by a factor of 100.
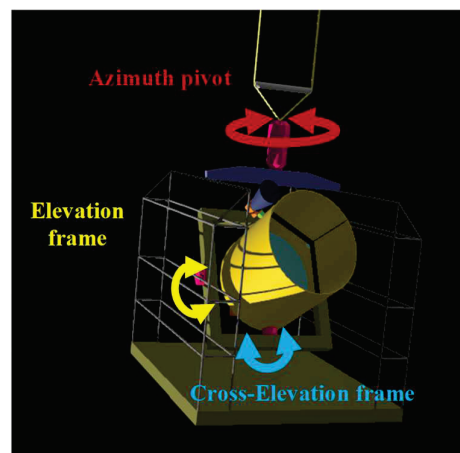

Figure 5. The first two stages of the DICOS pointing system

2.4 DICOS main technical requirements

Following a detailed analysis of the context and the results obtained on the CNES IHDC breadboard, we adopted the following technical goals:

- Pointing: 10 mas, 50 Hz bandwidth, 500 Hz sampling
- WFE: 20 nm rms WFE with 1 nm stability, Z4-Z36, 0.01 Hz sampling

This paper focuses on the second item. Another publication[15] is dedicated to the pointing issues.

3.   ACTIVE OPTICS IN DICOS

3.1 Some design choices

The foreseen general command sequence of the active instrument is:

- The M2 position is adjusted using an image of the brightest star on the guiding camera and a coarse algorithm,
- The position of the brightest star is evaluated on the guiding camera,
- The pointing command is offset to put the signal into the small FOV of the central channel using a flat mirror with a central hole,
- As soon as a signal is available on the fine pointing camera, the fast pointing loop starts (Z2-Z3),
- When the fine pointing is acquired, the slow AO loop is activated to correct the WFE (Z4-Z36).

The main idea is to stabilize the low frequency of the telescope WFE (Z4-Z36) while controlling the tip/tilt much faster using the same controlling device. This saves one mechanism and reduces the development efforts. We assumes that the WFE (Z4-Z36) variations are at very low frequency corresponding to the thermal fluctuations only and can be decoupled from the faster tip/tilt (Z2-Z3) fluctuations that are dominated by a 0.5 Hz 1'' 0-p residual from the second pointing stage. This is only true if the beam-walk effects are negligible. Also, µvibrations effects are not corrected and have to be minimized by the mechanical design.

The very fine pointing is implemented on board using real time software and computers, with a simple algorithm based on barycentering. The slower AO level uses the "ground in the loop" by sending the images to a ground control station. The optimum command is computed and sent back to the instrument. Implementing the AO algorithm in an on board electronics is technically feasible, but the cost is far beyond the DICOS budget.

The ALPAO DM97-25 was selected because:

- Its pupil size is well adapted to the telescope size with a ratio of about 20 with the M1 pupil size,
- The number of useful actuators matches the spatial frequency domain we want to correct with some margin,
- The large stroke is necessary to compensate for potentially high telescope deformation,
- The resolution is better than 1 nm,
- The temporal response is 1 ms, compatible with the implementation of the tip/tilt fast correction,
- Pre-qualification tests show it is compatible with future space use,
- The cost is affordable in the frame of the DICOS project.

For the AO wavefront sensing, we selected the phase diversity (PD) because it does not require an additional device (unlike a Shack Hartman) and a validated algorithm is already available at CNES requiring only slight modifications to adapt it to the DICOS case. One of the drawback is the relatively large computation time, but this is compatible with the targeted low sampling frequency for correcting Z4-Z36.

The first idea was to use the same camera for both the pointing and the phase diversity using two adjacent ROIs, but the difference in the required integration time to get the correct SNR is not compatible with the dynamical range of the selected camera and leads to a too complicated real time algorithm. That is why we use two cameras of the same type: CAM1 and CAM1B. The first one is for the pointing and operates with a 50 px ROI with 1 ms integration time. The second one is for the PD with an integration time varying from 20 to 200 ms. It is located the closest possible to the coronograph where the stabilization is required. We assume that there are no differential high frequency tip/tilt variations between the two locations. NB: low frequency tip/tilt variations can be estimated by the PD on CAM1B along with the other Zi.

The cameras are GT 1930 AVT Prosilica models using CMOS technology. We selected them because they are compatible with the existing balloon avionics and operating system, they have a very low RON, a high reading frequency and an adapted sensor size. The drivers from the ESTADIUS case can then be adapted easily. This reduces a lot the development efforts.

The 40 cm size with the selected spectral bands allow to reach a very good SNR for stars up to V=6 with 0.2 s maximal integration time for the PD and 1 ms for the very fine pointing.

3.2 The DM

The ALPAO DM97-25 can be seen on fig. 6 mounted on a Thorlabs KM-200PM mount and a MAX313 translation stage.
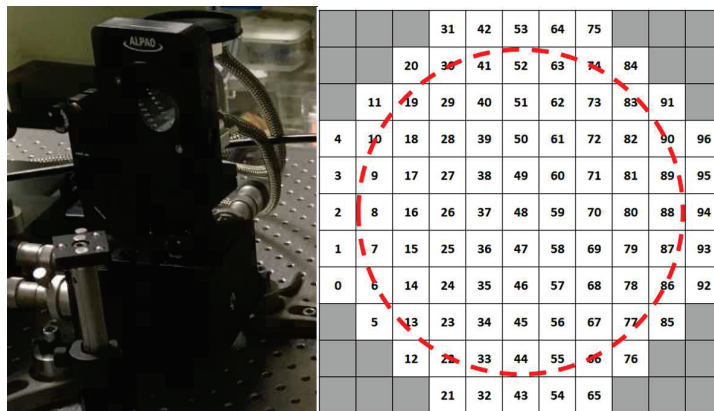

Figure 6. the ALPAO DM used for the WFE control and the very fine pointing

It uses 97 electro-magnetic actuators located just behind the mirror surface with a 2.5 mm spacing. The outer ring is not in the 22.5 mm optical pupil. The associated actuators have fixed mechanical interface on the outer edge and help to ensure the good transition with the central shape of the mirror. Although they are not visible, they must be included in the command to get appropriate shapes of the mirror. According to the data sheet, the non-linearity is lower than 3%, with an hysteresis lower than 2%. This is a limitation in our case. If too large commands are used to correct the tip/tilt, the hysteresis will create errors that can affect the correction on the other Zi of the WFE.

The driving electronics uses a Gigabit Ethernet card that allows sending commands at high rate and make a full use of the quick settling time (1.5 ms). It is adapted to ground use, but flying it under a stratospheric balloon will require some effort to reduce the power and adapt the cooling system, as fans are no more efficient at 40 km altitude.

ALPAO delivered the DM with a calibrated command matrix, called Z2C. Each column is a vector that corresponds to a Zernike polynomial from Z2 to Z97. As the PD algorithm also relies on the same formalism, the DICOS AO loop will naturally uses this decomposition of the WFE. There is no need to build an interaction matrix. The driving of the DM was implemented in a dedicated LabVIEW software for ground testing. It was checked with the DM in front of the Zygo to verify the Zi convention, signs and amplitude (see 4.1).

As the Z2C was characterized by ALPAO on a 22.5 mm diameter, the optical set up has to guarantee that the full DM pupil is illuminated. This means that the focal of M3 has to be carefully sized to fulfill this requirement whatever the uncertainties on the optical parameters and alignment of M1 and M2. The output optical pupil after M3 is then a bit larger than 22.5 mm (24.5 mm), which means a slight loss of signal (0.85 transmission).

The correction efficiency of the DM was estimated by coupling an optical model of the telescope and the DM properties in the CodeV software using routines developed in the frame of the OTOS/TANGO projects. Due to its limited sampling (9 actuators in the diameter, about 25 on the perimeter), the correction efficiency drops when the order of the polynomial is increased as shown on fig. 7. It drops much faster for the pure radial terms than for the azimuthal ones. For our initial goal to correct Z4-Z36, the predicted efficiency is above 80%, which is very good. In fact, we could probably extend to correction up to order 10 but for some terms only.
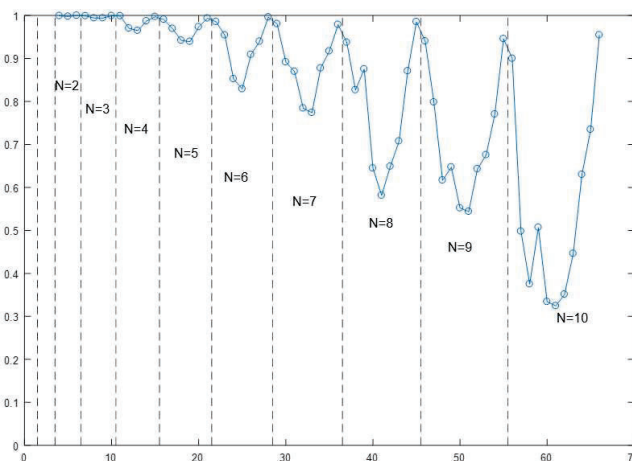

Figure 7. Predicted correction efficiency (%) as a function or Zernike index. N is the order of the Zi.

Using the same model and Monte-Carlo simulations taking into account reasonable WFE errors from alignment, thermal behavior and mirrors polishing, we could estimate that once the M2 has corrected the high initial defocus term, less than 10 % of the DM stroke is required to compensate the instrument defects in any case.

3.3 Phase diversity

Phase diversity principle

The wavefront metrology within DICOS AO loop is based upon a phase diversity algorithm[16], which has already proven to be efficient for space applications (HST[17], JWST commissioning phase[18], high-resolution Earth observation systems developed by CNES[19]). PD is based upon the use of at least two images of a source, each being acquired with a known

differential phase. Usually a differential defocus is used, as it can be easily induced through a displacement of the focal plane (or M2 mirror) along the optical axis. Through an accurate parametrical model of both the point source and the detection chain, PD algorithm may be used to recover the set of parameters (in particular Zernike modes) that best fit the observations.

Parametric model of broadband PSF

The detection chain is assumed linear and spatially invariant, meaning that the instrument may be fully characterized by its modulation transfer function (MTF) at a given wavelength λ. The MTF can then be considered as the multiplicative product of several contributors:

$$MTF(\lambda) = MTF_{opt}(\lambda) \times MTF_{det} \times MTF_{stab} \times MTF_{shift}$$

Each term represents respectively the optical model, the detector integration, the smearing effects due to instability during the integration time and the position shift within a pixel.

- Assuming far field Fraunhofer approximation,

$$MTF_{opt}(\lambda) = FT\left(\left| FT^{-1}\left(Pe^{j\frac{2\pi}{\lambda}WFE}\right)\right|^2\right)$$

  FT being the Fourier Transform. P is the occultation mask, considered binary unless amplitude attenuation occurs. The WFE is modeled as a sum $WFE = WFE_{HO} + \sum_{i\in\mathfrak{I}} \alpha_i Z_i$, where $\{\alpha_i\}_{i\in\mathfrak{I}}$ are the Zernike coefficients corresponding to the aberrations to be searched. WFE_{HO} represents the *a priori* knowledge of the WFE high-order aberrations measured on ground using interferometric measurements, assumed constant after launch.

- MTF_{det} is modelled through a *sinc* function $(sinc(f) = sin(\pi f)/\pi f)$, the Fourier transform of a top-hat function representing the pixel sampling. Charge diffusion effects can also be included as an additional *sinc*, such that:

$$MTF_{det}(\lambda) = sinc(af_x)sinc(bf_y)sinc(a_{diffusion}f_x)sinc(b_{diffusion}f_y)$$

  where a, b refer to the photosensitive detector dimensions, $a_{diffusion}$, $b_{diffusion}$ to the diffusion parameters. It should be noted that these diffusion parameters could be wavelength dependent. This component can be calibrated on the ground and considered constant in flight.

- MTF_{stab} may be modelled using a Gaussian kernel, the Fourier transform of a AOCS time series or once more using a *sinc* function for a constant velocity displacement during the integration time.

- Finally, exact location of the pointwise source has to be taken into account through a linear ramp phase in the Fourier domain:

$$MTF_{shift}(f_x, f_y) = exp\left(2\pi j\left(f_x d_x + f_y d_y\right)\right)$$

  with $\left(d_x, d_y\right)$ being the vector joining the exact point source position and the center of the acquired image.

By returning the MTF into detector space, we obtain a parametric estimate of $PSF(\lambda)$. This model is expanded to the entire spectral bandwidth of the instrument by integrating the previous expression over λ accounting for the star spectral energy density (SED) and the overall transmission/quantum efficiency of the system. The broadband PSF is in practice computed using only a handful of monochromatic MTFs, with the number of wavelength depending on the spectral bandwidth and the targeted accuracy. By definition, the PSF is normalized to a unit integral, so that the final model used for PD is:

$$Model = A \times PSF + offset$$

where A and offset are two unknown parameters, respectively linked to instrumental absolute calibration factor (and the star flux) and offset refers to dark current residuals. This model is often created on an oversampled grid to properly simulate aliasing, and is therefore undersampled and cropped to match the observed tile around the star in the PD algorithm.

Algorithmic implementation, complexities and way forward

The PD algorithm minimizes a weighted quadric distance between the model M and observation O in the detector space:

$$(p1, p2, \dots pn) = argmin\left(\sum_{pixels\ i,j} \left|\frac{O(i,j) - M_{p1,p2,\dots pn}(i,j)}{\sigma_{i,j}}\right|^2\right)$$

$\sigma_{i,j}$ is the noise standard deviation of pixel (i,j), modelled as $\sigma_{i,j} = \sqrt{\alpha^2 + \beta model_{p1,p2,...pn}(i,j)}$, with (α,β) known parameters. Such a ponderation allows giving less importance to noisy pixels. The minimization is achieved using a Levenberg-Marquart (LM) descent algorithm[20]. The defocused model follows the same rules, except that a $\alpha_4 Z_4$ contribution is added to the WFE, with α_4 being the RMS value of the differential defocus. This additional acquisition is theoretically mandatory to get rid of the ambiguity of the sign of the WFE symmetrical component in the minimization, whenever the pupil mask P is symmetrical. In practice, it also increases the robustness of the technique. PD efficiency finally depends on the number of unknown variables versus the number of pixels observed (with significant SNR).

The algorithm complexity is linked to the number of PSF models generated. At each iteration, the LM algorithm needs a Jacobian matrix computation, which means generating as many PSF models – potentially broadband – as the number of unknown variables. Fast FT algorithms are called many times and an efficient version must be used. To match this complexity, parallelization and Hermitian symmetry of real function Fourier transform is systematically exploited. In the case of DICOS, only monochromatic point sources were considered. Further, the ratio between the CMOS Nyquist frequency and the optical cut off frequency meets the Shannon requirement, which implies the PSF model dos not need to be oversampled. Monochromatic model directly created at pixel step size is therefore sufficient, which is beneficial both for the overall complexity of the algorithm (no broadband integration) and for its runtime. Last, the size of the pupil sampling was optimized (128 x 128) to improve again the runtime.

These techniques have been deepened for OTOS studies[1] where active optics on board future very high-resolution systems have been envisaged. CNES involvement in the preparation of the EUCLID project have also brought significant improvement in runtime, number of useable observations and model complexity. The high WFE stability required for DICOS (< 1 nm), is an ideal case of application, as it drives its runtime. Number of other optimizations are currently under study to accelerate the PD. Interestingly for DICOS, once the first major aberration corrections are done, the AO loop should only correct small aberration changes. This means that only a few iterations for the LM algorithm – possibly one or two – may suffice. Linear expansions of the PD problem may also be planned, and will be investigated in future analysis.

4. DM CHARACTERIZATION AND TESTS

4.1 Set up

In 2021, the DM97-25 procured in the frame of the DICOS project was installed in front of a Zygo (Verifire Z-series) available in the CNES optical laboratory. A LabVIEW based program allowed to send individual commands on each Zi based on an interaction matrix provided by ALPAO. The rms sent value is then compared to the measurement provided by the Zygo (SFE, integration time 20 ms). The environment is a classical ISO8 laboratory with 1°C thermal control and humidity at the 50 +/- 5% level. Fig. 8 gives the measured fluctuations of each Zi due to the turbulence in the set up. The turbulence classically affects more the low order terms with up to 0.2- to 0.5 nm standard deviation, except for the tip/tilt that can reach up to 3 nm rms standard deviation here. The impact on terms higher than Z11 is lower than 0.1 nm rms standard deviation. The standard deviation on the rms value is 0.25 nm after averaging (tip/tilt removed).
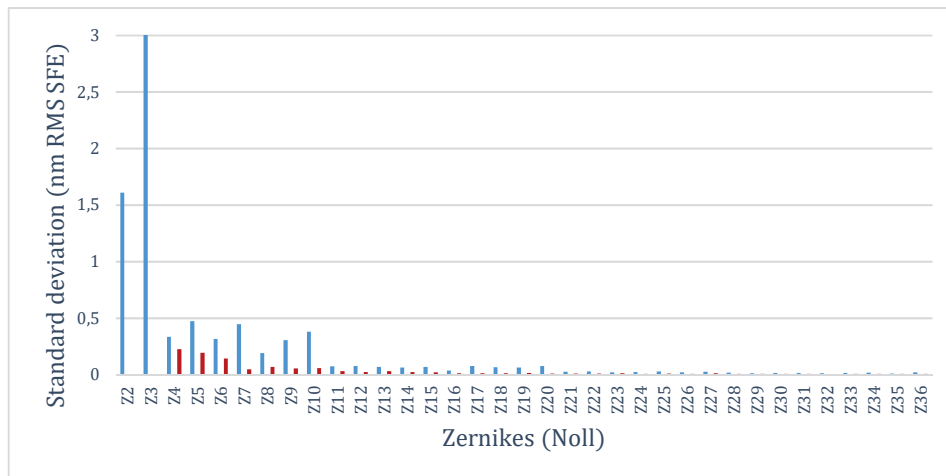

Figure 8. Turbulence measurements. Blue: 20 measurements of 20 ms, no averaging. 20 measurements with averaging on 10 frames.

4.2 Linearity and hysteresis

For each Zi up to 16, we sent the following SFE commands: +100 nm rms, back to 0, -100 nm rms, and back to 0. The linearity is excellent, but some hysteresis appears. Fig. 9 gives the ratio of the measured hysteresis to the applied command. We found values from 1 to 4%. On average, we have 2.5% quite consistent with the ALPAO datasheet. This expected behavior comes from the electro-magnetic actuators used in the DM. To check the possible impact of Z2-Z3 hysteresis on the higher Zi, we tested a 0, 500 nm rms, 0, -500 nm rms (WFE) sequence on Z2 and Z3 in front of the Zygo and measured the impact on the WFE up to Z36. 500 nm rms corresponds to the expected stroke of the fine pointing for DICOS. We found an impact lower than 0.6 nm on the WFE rms value that is then compatible with our stability goal.
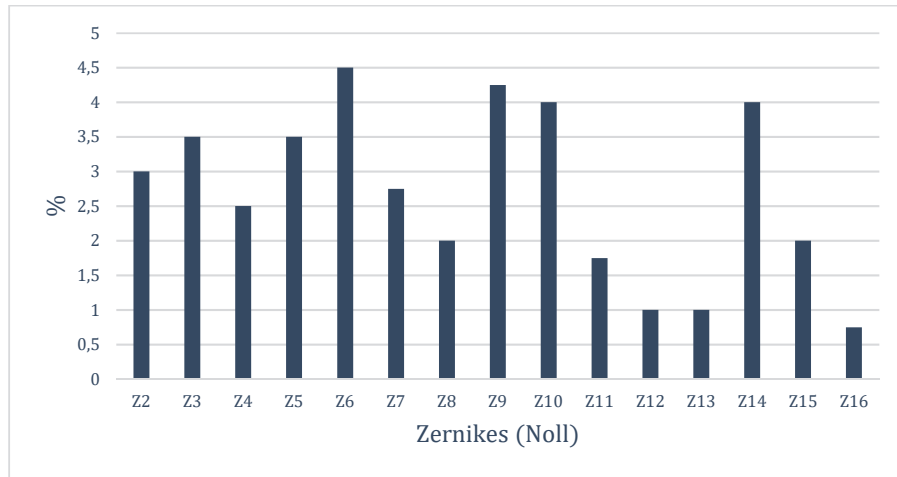

Figure 9. Measured hysteresis up to Z16

4.3 Best flat

Adjusting directly the 7 first orders leads to a first flat map with less than 10 nm rms (SFE) residuals quite easily (see fig. 10). As said previously, the DM allows correcting some higher orders with azimuthal variations but this requires an automated procedure, which was not available at the time of this measurement. From the delivered documentation, the best performance is 5.8 nm rms (SFE), quite consistent with our measurement given our limitation to the 7th order. We are then quite confident that this DM can reach our 20 nm rms goal on the WFE.
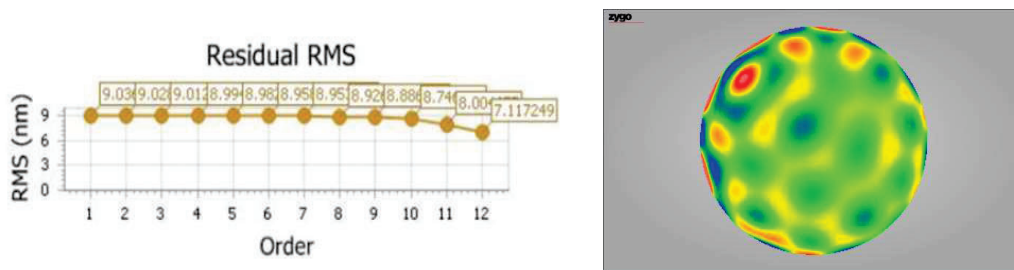

Figure 10. First flat map obtained in front of the Zygo

4.4 Stability

The DM is started and a flat map with less than 10 nm rms SFE is sent. Regular measurements from the Zygo show the stability in open loop (see fig. 11). One can observe a settling time of about 30 to 40 minutes corresponding to the temperature stabilization of the DM and its driving electronics. The evolution after 1 h comes from the drift of the temperature inside the laboratory.
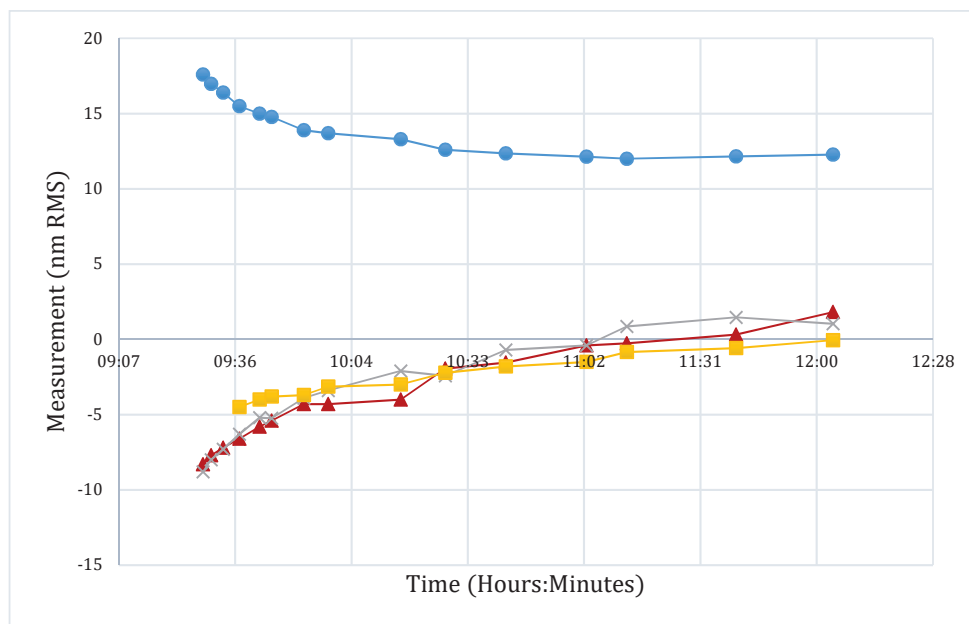
Figure 11. Stability of Z4 (red, triangle), Z6 (gray, cross), Z7 (yellow, square), and rms (blue, dot, up to Z_{36}) after starting the DM

4.5 Environmental tests

First, a DM97-15 resisted a 50 g mechanical environment without any impact on its properties. Second, ADS and ALPAO performed a thermal-vacuum test under a CNES contract. In a first part, a stabilized version of the DM97-15 was exposed to high vacuum with small temperature variations. The facility had a window to control optically the influence functions during all the test duration using a Fizeau interferometer. The differences between air and vacuum are less than 1.5 % and the impact of the temperature on the influence function is negligible within the tested range (few °C around 22°C). In a second part, the DM (in off mode) was exposed to eight [-15, 50°C] thermal cycles under air with N_2 flushing simulating non operational conditions. A detailed control of its properties before and after the tests shows that there are no measurable variations of the DM behavior.

5. EXPERIMENTAL RESULTS OF THE AO LOOP

5.1 Set up description

Fig. 12 shows the set up used in the CNES optical laboratory to test the properties of the AO loop. The source is a monochromatic DFB laser at 637 nm collimated by a f=500 mm lens. The entrance pupil is made by a circular diaphragm with 6.75 mm diameter and μm precision on the circularity. The non-uniformity due to the Gaussian distribution is less than 1% as only the center of the beam is selected. A simple lens (L1) and an off axis mirror (M3) forms an afocal that conjugates the diaphragm and the DM. The diameter of the beam is larger than the 22.5 mm real pupil of the DM to make sure it is fully illuminated as previously explained. The M4 off-axis parabola focuses the beam on a GT 1930 camera and the sampling is close to 4 px per airy radius. M3 and M4 are on the shelf optics with properties as close as possible to the DICOS ones as the real optics are not yet available. The focal length are within 5 %, but the off axis angle is twice (15° vs 7.5°) and the WFE is much worse (150-200 nm rms rms vs 50 nm rms). The setup is then a first approximation of the central part of fig. 4 with worst case optics. CAM1 is mounted on a MTS25 motorized translation stage to inject the differential phase between the two images required for the PD. Given the optical parameters, a 1 mm translation creates a 42 nm rms defocus (Z4).
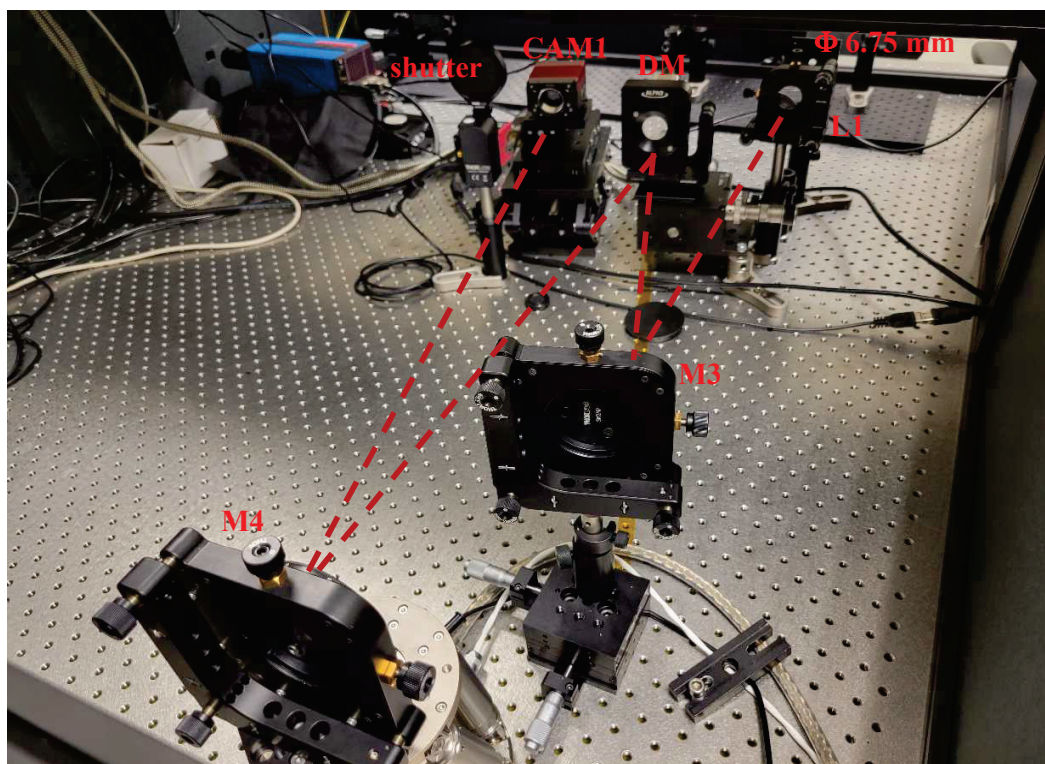
Figure 12. Laboratory set up

A LabVIEW software drives the camera (via NI vision tools), the DM (specific development based on the Z2C matrix), the translation stage, the shutter. The PD algorithm is implemented under Linux. The AO loop can be closed using two parallel asynchronous processes. The LabVIEW sequence takes first dark images using the shutter, then two images for the PD by moving the translation stage with the appropriate displacement. The PD algorithm starts a new loop as soon as new images are stored. This loop creates a file with the measured Z_i. The Labview code takes each new Z_i file, computes a correction just by sign inversion and use of the Z2C matrix and apply it to the DM. Each iteration takes about 40 s with identification up to Z36. The integration time is 50 ms and the power of the DFB is adjusted to get the image at best focus with about 60-70 % of the maximum allowed (3000 adu for 4096, 12 bits). An averaging of 10 images is performed. The ROI is 50 pixels wide. The breadboard has a cover with 30 cm height to limit the turbulence to a level about 2-3 times better than in fig. 8.

5.2 Results on the AO loop

Acquisition

We performed an extensive experimental study to estimate how bad can be the initial WFE so that the PD algorithm can start without diverging or producing wrong results. This is quite important as this drives the M2 alignment precision that has to be reached by moving the hexapod and beyond the tolerances of the optics and of the structure. First, we tested the acquisition limit for each Z_i up to 11. Using a 70 nm or 140 rms phase difference on Z4, and a 20 nm rms increment on the error, we obtain table 1. The obtained values are quite high. The PD can cope with quite degraded images with low SNR. Doubling the differential phase improves the limits but not proportionally and not in all cases.

In a second step, we simulated WFE errors representative of the telescope alignment and polishing errors using a Monte-Carlo analysis in a Zemax model. 10 cases were extracted and injected on the DM as initial errors on top of a flat map with a rms level of 200 to 600 nm rms dominated by low frequency terms (defocus, astigmatism, coma). We find that that the acquisition is possible up to at least 500 nm rms WFE with $\Delta\varphi$=70 nm rms on Z4. We will adopt this value for the goal of

the alignment procedure involving M2. This result is quite consistent with the estimations found in other projects like TANGO.

Zernike	Δφ=68 nm rms	Δφ=140 nm rms
Z4	650	800
Z5	140	300
Z6	180	280
Z7	100	80
Z8	120	80
Z9	80	160
Z10	80	120
Z11	100	140

Table 1: Bounds on initial WFE to perform PD acquisition

Convergence

The convergence of the AO loop is illustrated by fig.13. In this cases, the initial WFE was close to 530 nm rms and we used Δφ=140 nm rms on Z4 for the PD. The most efficient strategy was found to alternate steps with Z4-Z11 and Z4-Z36. Each step last 40 s. The first step improves the WFE by a factor of 10 only correcting Z4 to Z11.
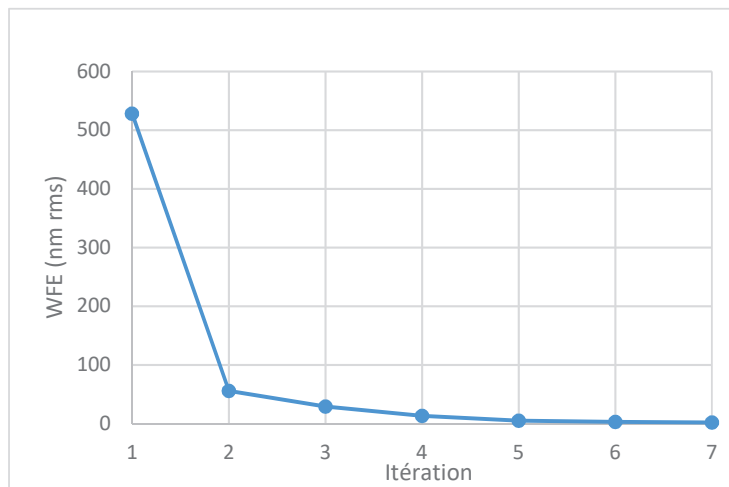
Nb de Zernike	WFE tot (nm rms)
11	528,23
	56,04
36	29,36
	13,07
11	6,55
	1,42
36	5,19
	3,03
	1,91

Figure 13. Example of convergence starting from a high initial WFE

After 3 steps correcting Z4-Z36 it was found necessary to perform another correction with low frequency again to optimize the convergence. The final result is close to 2 nm rms which is excellent. A detailed analysis of the residual shows that we are mainly limited by the turbulence. Similar curves were made for lower initial WFE. For 100 nm rms, only 1 step is required to go below the 20 nm rms requirement.

This experimental results proves that the AO based on the PD can cope with the expected initial errors and maintain the WFE below 20 nm rms with better than 100 s period. This is a key point for DICOS.

5.3 Stability on 24h

Fig. 14 shows the evolution of the rms WFE (Z4-Z21) in open loop during 24h, as measured by the PD with ~40 s steps, along with the measured temperature in the laboratory. The first hour correspond to the stabilization time of the DM as already explained. After that, we observe few nm fluctuations directly correlated with the temperature and a small drift of less than 0.1 nm/h. The variations are dominated by defocus and astigmatism. Fig. 15 shows the same kind of measurement

but in closed loop. The rms is stabilized to better than 1 nm rms (0.7 nm on average, std dev = 0.13 nm) despite the temperature fluctuations.
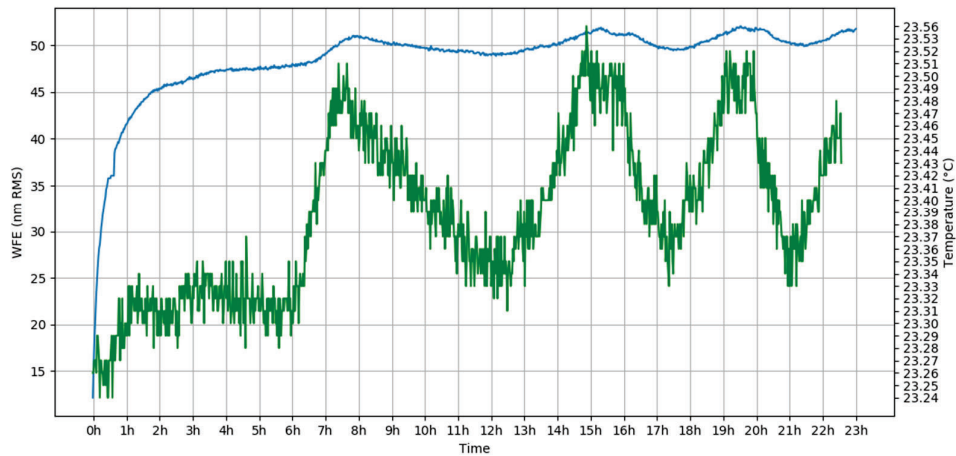

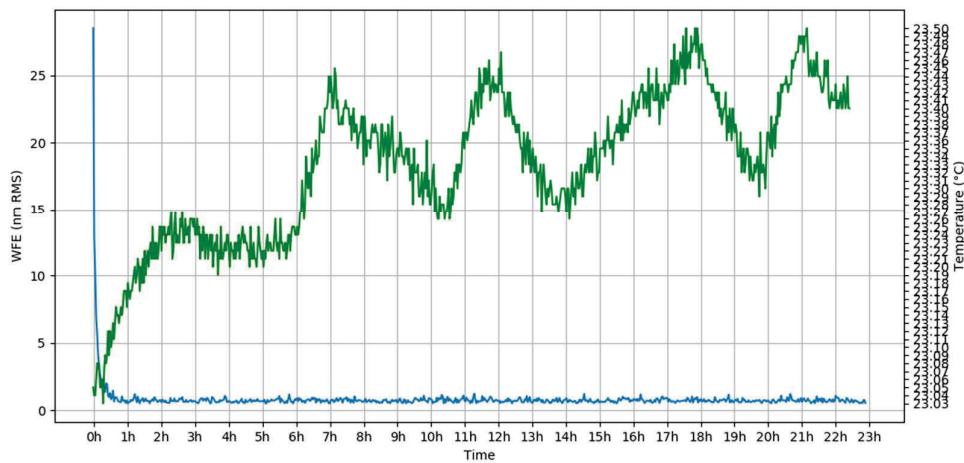Figure 14. variations of the rms WFE (Z4-Z21) over 24 h in open loop

Figure 15. variations of the rms WFE (Z4-Z21) over 24 h in closed loop

6. CONCLUSION

This experimental work performed since 2019 at CNES provides a strong basis for the AO of the DICOS project. The ALPAO DM97-25 and the CNES PD algorithm form a powerful combination that can accept as much as 500 nm rms initial WFE and reach a few nm residual on Z4-Z36 terms with better than 40 s correction period. The first pre-qualification tests show that the DM is compatible with vacuum and large thermal variations. In late 2022, we plan to implement this AO loop on the optical bench with the real optics that are currently in the manufacturing phase. The optical bench will be coupled with the telescope mid 2023. We expect a full on-ground demonstration of the project including the fine pointing stage by the end of 2024.

REFERENCES

[1] V. Costes, L. Perret, D. Laubier, J. M. Delvit, C. Imbert, et al., "Active optics for next generation space telescopes", Proc. SPIE 10398, 103980S (5 September 2017)

[2] R. Cousty, T. Antonini, M. Aubry, H. T. Krol, et al. "Monomorph deformable mirrors: from ground-based facilities to space telescopes", International Conference on Space Optics, Biarritz, France, 18–21 October 2016

[3] Marie Laslandes, Claire Hourtoule, Emmanuel Hugot, Marc Ferrari, Christophe Devilliers, Arnaud Liotard, Céline Lopez, Frédéric Chazallet, "Last results of MADRAS, a space active optics demonstrator," Proc. SPIE 10564, International Conference on Space Optics — ICSO 2012, 1056413 (20 November 2017);

[4] Ch. Latry, J. M. Delvit, C. Thiebaut, "Sensitivity analysis of phase diversity technique for high resolution earth observing telescopes", Proceedings Volume 10562, International Conference on Space Optics — ICSO 2016

[5] D. Sucher, G. Butel, G. Briche, J.-F. Blanc, A. Liotard, et al., "Active optics for space telescopes", Proc. SPIE 11116, Astronomical Optics:Design, Manufacture, and Test of Space and Ground Systems II, 1111611 (2019)

[6] P. Baudoz, R. Galicher, A. Potier, O. Dupuis, S. Thijs, F. Patru, "Optimization and performance of multi-deformable mirror correction on the THD2 bench", Proc. Of SPIE Vol. 10706 (2018)

[7] D. Rouan, P. Riaud, A. Boccaletti, Y. Clénet, A. Labeyrie, "The Four-Quadrant Phase-Mask Coronagraph. I. Principle", Publication of the ASP, 112:1479-1486 (2000)

[8] R. Galicher, P. Baudoz, G. Rousset, J. Totems and M. Mas "Self-coherent camera as a focal plane wavefront sensor: simulations," Astronomy and Astrophysics 509, A260000+ (2010).

[9] J.M. Le Duigou et al " DICOS: a demonstrator of advanced active optics and fine pointing techniques for future space based missions", Proc. Of SPIE Astronomical Telescopes and Instrumentation, Montreal, 2022

[10] V. Dubourg; A. Vargas; P. Cocquerez ; P. Raizonville ; S. Louvel, " French balloon activities 2018-2021: national report », 43rd COSPAR Scientific Assembly. Held 28 January – 4 February, 2021

[11] K. Hoadley et al., "The FIREBall-2 UV balloon telescope: 2018 flight and improvements for 2020", UV, X-Ray, and Gamma-Ray Space Instrumentation for Astronomy XXI, Proc. of SPIE Vol. 11118 (2019)

[12] M. Matuszewski et al. "FIREBALL: Instrument pointing and aspect reconstruction", Proc. SPIE. 7732, Space Telescopes and Instrumentation 2010: Ultraviolet to Gamma Ray

[13] J. Montel et al. , "FIREBALL-2 (2018) in flight performances, ESA PAC 2019

[14] J. Montel et al., "ESTADIUS: A High Motion "One Arcsec" Daytime Attitude Estimation System for Stratospheric Applications", Proc. of the 22nd ESA Symposium on European Rocket and Balloon Programs and Related Research, Tromso, Norway (2015)

[15] C.A. Chevrier "Attitude control system architecture of the DICOS mission : ambitious sub arcsec pointing using adaptative optics", 25th ESA PAC Symposium – Biarritz, France (2022)

[16] R.A. Gonsalves, "Phase diversity: math, methods and prospects, including sequential diversity imaging," Proc. SPIE 10677, Unconventional Optical Imaging, 106771S (24 May 2018);

[17] J.R. Fienup, J. C. Marron, T. J. Schulz, and J. H. Seldin, "Hubble Space Telescope characterized by using phase-retrieval algorithms," Appl. Opt. 32, 1747-1767 (1993)

[18] B.H. Dean, David L. Aronstein, J. Scott Smith, Ron Shiri, D. Scott Acton, "Phase retrieval algorithm for JWST Flight and Testbed Telescope," Proc. SPIE 6265, Space Telescopes and Instrumentation I: Optical, Infrared, and Millimeter, 626511 (13 June 2006);

[19] V. Amberg, L. Bernard, C. Latry, "Star-based defocus computing technique for PLEIADES-HR satellites," Proc. SPIE 9643, Image and Signal Processing for Remote Sensing XXI, 964303 (15 October 2015);

[20] Moré, J.J. (1978). The Levenberg-Marquardt algorithm: Implementation and theory. In: Watson, G.A. (eds) Numerical Analysis. Lecture Notes in Mathematics, vol 630. Springer, Berlin, Heidelberg.